Advances in Nano Research, *Vol. 16, No. 2 (2024) 127-140*
https://doi.org/10.12989/anr.2024.16.2.127

Optimal flammability and thermal buckling resistance of eco-friendly abaca fiber/ polypropylene/egg shell powder/halloysite nanotubes composites

Saeed Kamarian*[1], Reza Barbaz-Isfahani[2], Thanh Mai Nguyen Tran[1,3], and Jung-Il Song**[1]

[1]*Department of Mechanical Engineering, Changwon National University, Changwon, South Korea*
[2]*Department of Mechanical Engineering, Amirkabir University of Technology, Tehran, Iran*
[3]*Faculty of civil engineering, Nha Trang University, Nha Trang-650000, Vietnam*

(*Received May 1, 2023, Revised June 21, 2023, Accepted July 31, 2023*)

Abstract. Upon direct/indirect exposure to flame or heat, composite structures may burn or thermally buckle. This issue becomes more important in the natural fiber-based composite structures with higher flammability and lower mechanical properties. The main goal of the present study was to obtain an optimal eco-friendly composite system with low flammability and high thermal buckling resistance. The studied composite consisted of polypropylene (PP) and short abaca fiber (AF) with eggshell powder (ESP) and halloysite clay nanotubes (HNTs) additives. An optimal base composite, consisting of 30 wt.% AF and 70 wt.% PP, abbreviated as OAP, was initially introduced based on burning rate (BR) and the Young's modulus determined by horizontal burning test (HBT) and tensile test, respectively. The effects of adding ESP to the base composite were then investigated with the same experimental tests. The results indicated that though the BR significantly decreased with the increase of ESP content up to 6 wt.%, it had a very destructive influence on the stiffness of the composite. To compensate for the damaging effect of ESP, small amount of HNT was used. The performance of OAP composite with 6 wt.% ESP and 3 wt.% HNT (OAPEH) was explored by conducting HBT, cone calorimeter test (CCT) and tensile test. The experimental results indicated a 9~23 % reduction in almost all flammability parameters such as heat release rate (HRR), total heat released (THR), maximum average rate of heat emission (MARHE), total smoke released (TSR), total smoke production (TSP), and mass loss (ML) during combustion. Furthermore, the combination of 6 wt.% ESP and 3 wt.% HNT reduced the stiffness of OAP to an insignificant amount by maximum 3%. Moreover, the char residue analysis revealed the distinct differences in the formation of char between AF/PP and AF/PP/ESP/HNT composites. Afterward, dilatometry test was carried out to examine the coefficient of thermal expansion (CTE) of OAP and OAPEH samples. The obtained results showed that the CTE of OAPEH composite was about 18% less than that of OAP. Finally, a theoretical model was used based on first-order shear deformation theory (FSDT) to predict the critical bucking temperatures of the OAP and OAPEH composite plates. It was shown that in the absence of mechanical load, the critical buckling temperatures of OAPEH composite plates were higher than those of OAP composites, such that the difference between the buckling temperatures increased with the increase of thickness. On the contrary, the positive effect of CTE reduction on the buckling temperature decreased by raising the axial compressive mechanical load on the composite plates which can be assigned to the reduction of stiffness after the incorporation of ESP. The results of present study generally stated that a suitable combination of AF, PP, ESP, and HNT can result in a relatively optimal and environmentally friendly composite with proper flame and thermal buckling resistance with no significant decline in the stiffness.

Keywords: abaca fiber; cone calorimeter test; dilatometry test; eco-friendly composites; egg shell powder; halloysite nanotubes; horizontal burning test; polypropylene; tensile test; thermal buckling analysis

1. Introduction

As worries about environmental impacts of consuming hard-to-degrade products escalate, more and more researchers/ practitioners are considering the industrial use of eco-friendly materials in different sectors (Kamarian and Song 2022). Thanks to their low cost, biodegradability, light weight, and wide availability, natural fibers (NFs) have been widely utilized to develop different composites for a variety of industries (*e.g.*, automotive industry, railway infrastructures, construction industry, home and office furniture, etc.).

Of the pool of commercially available NFs, the AF has been the choice for synthesizing countless NF composites. Extracted from the Musa textilis (*i.e.*, a plant) (Ochi 2006), AF is dominantly produced in the Philippines wherein 84% of total demand for the abaca around the globe is being supplied at an annual average rate of 68,000 t/year (Barba *et al.* 2020). In terms of appearance, the abaca plant looks like a banana tree in that it has a root system in the middle from which 12–30 stems are originated. Growing to up to 8 m, the stems (*i.e.*, stalks) are peeled to obtain AF. With lengths in the range of 1.5–3.5 m, the AFs exhibit various colors ranging from white to red and then to brown and black or purple (Vijayalakshmi *et al.* 2014). Being a highly strong commercially available NF, AFs have found diverse applications. The ever-increasing industrial application of AF as a sustainable source of fiber is associated with its

*Corresponding author, Ph.D.,
E-mail: kamarian@changwon.ac.kr,
kamarian.saeed@yahoo.com
**Co-corresponding author, Ph.D.,
E-mail: jisong@changwon.ac.kr

ISSN: 2287-237X (Print), 2287-2388 (Online)

acceptable mechanical strength coupled with long durability, high flexibility and resistance to saltwater, favorable buoyancy behavior, and adequate length of the fibers. Basically, AF is composed of cellulose (~60%) with minor amounts of hemicellulose (~21%), lignin (~12%–16%), and pectin (~1%) (Sun *et al*. 1998). The high strength and stiffness of AF, compared to other NFs, are known to be related to its high Runkle ratio (Liu, K. *et al*. 2013) and cellulose-to-hemicellulose and lignin ratio (Vijayalakshmi *et al*. 2014) alongside a microfibril angle that is close orienting along the fiber bundle (Madsen and Gamstedt 2013). Many recent studies have elaborated on the application of AF as reinforcement in various composites, thoroughly evaluating the behavior of the AF under different loading schemes (*i.e*., bending (Vijaya Ramnath *et al*. 2014), tensile (Vasquez and Diaz 2017), compressive (Manickavasagam *et al*. 2014), impact (Shaik and Subramanian 2021, Vijaya Ramnath *et al*. 2014), and thermal (Li *et al*. 2017) loading).

As a byproduct of poultry, chicken eggshell is known to seriously pollute the environmental around the world. It has a tri-layer structure where an intermediate spongy layer is coated with an outer layer of cuticle and an inner shell (Kang *et al*. 2010). Chemically describing an eggshell, it is reportedly composed of calcium carbonate (~94 wt.%) together with minor amounts of magnesium carbonate (~1 wt.%), calcium phosphate (~1 wt.%), and organic matter (~4 wt.%) (Tsai *et al*. 2006). According to the literature, eggshells can serve as biofiller in PP composites to cut the corresponding demand for talc and $CaCO_3$ by up to 75%. At the other end of the spectrum, this apparently waste material has been regarded as an eco-friendly catalyst, a bio-stabilizer for bone tissues, an adsorbent for particular metal contaminants, and a precursor for fabricating microporous CaO, among other advanced applications (Jena and Sahoo 2019, Jirimali *et al*. 2018, Xu *et al*. 2019).

With the chemical formula $Al_2Si_2O_5(OH)_4.2H_2O$, the HNTs represent a nano-sized class of kaolin clays that are composed of two-layer structures of Al, Si, H, and O. With their highly porous nature, HNTs have served as reinforcement for plastic composites (Deng *et al*. 2008, Liu *et al*. 2008) and particular medical and biological uses (Massaro *et al*. 2017, Santos *et al*. 2018). In particular, studies have highlighted the applicability of HNTs as nanofiller, even at dosages as low as 3–6 wt.%, to achieve remarkable improvements in compressive modulus and strength as well as thermal stability (Liu *et al*. 2013, Naumenko *et al*. 2016).

Globally known as a highly popular base polymer, PP is obtained by catalyst-assisted polymerization of the propylene under relatively mild conditions in terms of pressure and temperature (Busico and Cipullo 2001, Maddah 2016, Shubhra *et al*. 2013). The wide applications of PP, especially in fiber and plastic industries, root in its versatile characteristics. A distinctive feature of PP, as compared to conventional polymers like polyamides, comes in the face of the fact that it does not absorb moisture, making it an alternative of choice for numerous applications. Furthermore, post-synthesis modifications can be applied to further enhance the PP properties.

Natural composites are known to come with particular disadvantages that can partly underpin their significant benefits. Most importantly, these composites are known to exhibit relatively poor mechanical performance and be highly flammable and moisture-absorbing. To address these disadvantages, researchers have introduced HNTs, ammonium polyphosphate (APP), magnesium hydroxide (MH), and ESP, among other additives, to modify NF composites (Balan *et al*. 2020, Kamarian *et al*. 2022). Investigating AF-reinforced composites, Li *et al*. (2017) evaluated the impacts of combining nanoclays (NCs) with HNTs and APP on AF/vinyl ester composites in terms of thermal stability, flammability, and mechanical performance, ending up concluding that introducing the additives at optimal dosage can improve the synthesized composite in terms of fire resistance while slightly degrading its bending and tensile strengths. In another piece of research, Nguyen Tran *et al*. (2021) used ESP as a biowaste material to modify an AF/PP composite and checked the resultant changes in mechanical performance and fire resistance of the product. Preparing composite specimens through injection molding, they based their analyses on various tests (*e.g*., bending, tensile, and horizontal burning experiments). Findings suggested that the ESP can be utilized to improve fire resistance although it may lower the mechanical performance of the composite. Li *et al*. (2013) presented a work where they tried to figure out how NCs affect the tensile behavior and fire resistance of short AF/PP composites and ended up reporting significantly improved tensile behavior and fire resistance by incorporating the NCs at an optimal dosage.

In practice, composite structures may be exposed to flame or high-temperature environments encountered in particular applications (Carrera *et al*. 2016, Eslami 2010), in which case some destructive effects may render inevitable. Depending on the type of composite and the working conditions, burning (Mouritz and Gibson 2007, Qiu *et al*. 2022, Renner *et al*. 2021) or thermal buckling (Behdinan and Moradi-Dastjerdi 2022, Dai and Safarpour 2021, Shan and Huang 2022) may occur. The NF-made composites are even more sensitive to such harsh conditions due to the significantly weaker fire resistance and mechanical performance of the NFs, as compared to the synthetic fibers (Chalapathi *et al*. 2022, Kamarian *et al*. 2022).

The present research is motivated by lack of studies where burning and thermal expansion/thermal buckling of PP/AF composites are investigated simultaneously. The main objective of the present research is to introduce an optimal eco-friendly composite system that is adequately resistant to flame and thermal buckling. First, optimum content of AF was obtained for AF/PP composites by performing a series of preliminary fire tests, namely HBT for determining the BR, and tensile test for Young's modulus. Then, the effects of adding ESP at different content ranging from 0 to 6 wt.% on the flammability and stiffness were investigated. In order to compensate for the destructive effects of ESP on the mechanical properties, a small amount of HNT (3 wt.%) was further added to the AF/ PP/ESP composite. Next, CCT and dilatometry test (DT) were conducted for detailed investigation of fire-resistance and CTE of the proposed optimal composites. Finally, given the thermo-mechanical properties, an FSDT-

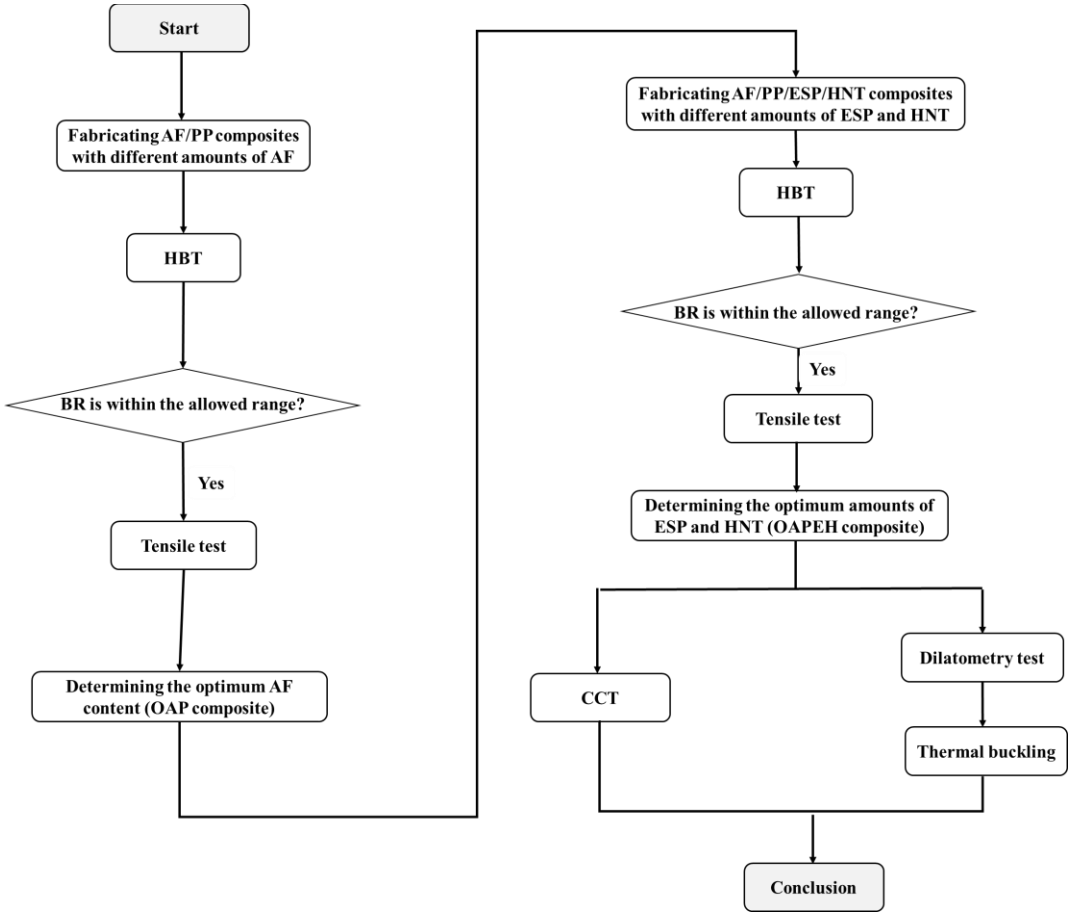

Fig. 1 The workflow of the present study

based theoretical model was used to analyze the critical buckling temperatures of the proposed composite system. The workflow of the present study is shown in Fig. 1.

2. Materials and methods

2.1 Preparation of eco-friendly AF/PP/ESP/HNT composite specimens

This section is devoted to describing the preparation of AF/PP composite samples with HNT and ESP additives. AFs were first cut into short fibers and mixed with PP. The mixture was dried in an oven at 60 °C overnight. Subsequently, the mixture of short AFs, PP (Chemko S.C.Corp., South Korea), HNT, and ESP (Edentown F&B, Poonglim Industrial Co. Ltd, South Korea.) was transferred into an extruder (SJZS-10B, Wuhan Ruiming Experimental Instrument Manufacturing Co., Ltd., China) where it passed a path with four different temperature zones (175, 180, 185, and 190 °C). Upon exiting the extruder, the molten composite passed over a conveyor exposed to a cooling system as a filament. After cooling down to room temperature the filament was inserted into a miniature granulator where it was converted into same-sized pellets. The process of extrusion and conversion into uniform pellets was repeated once more to reach higher homogeneity The AF/PP/ESP/HNT composite pellets were then transferred in a mold followed by hot pressing at 180 ℃ and pressure of 7 MPa. The composite sheets were then cooled to room temperature. The sheets were ultimately cut into suitable dimensions for the HBT, CCT, dilatometry test and tensile test. Fig. 2 illustrates the manufacturing process of PP/AF/ESP/HNT composites.

2.2 Experimental tests

2.2.1 Horizontal Burning Test

The HBT standard was carried out according to standard of the testing procedure detailed in the UL-94 utilizing a portable igniter. This test serves as preliminary indicator of acceptable flammability for a specific application (Karunakaran *et al*. 2016). The dimensions of the specimens were 125 × 12.5 × 3 mm^3. The BR, dripping time, and flame propagation of the sample can be determined by this method based on the first reference to the second reference marks which are at 25 mm and 100 mm from the end of the sample. Fig. 3 demonstrates the experimental setup as well as the relevant dimensions. The sample was clamped on the retort stand and flame was applied for 30 ±1 s at a transverse axis with 45 ±2° inclination relative to the free end of samples. The burner was eliminated after 30 ±1 s or when the combustion front of the specimen reached the 25 mm mark (Karunakaran *et al*. 2016). The timing device was

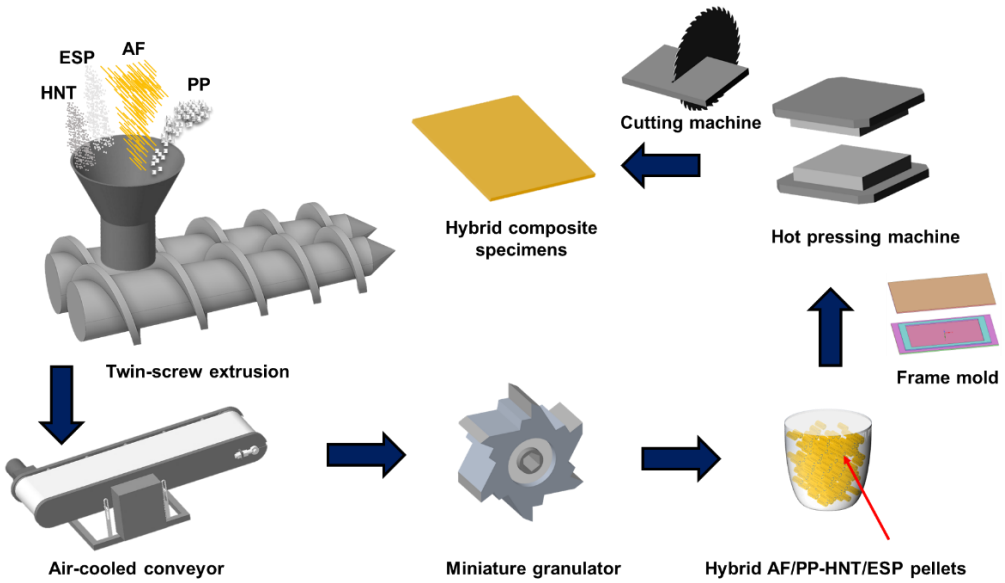

Fig. 2 Schematic of manufacturing of AF/PP/ESP/HNT composites using extruder–compression process

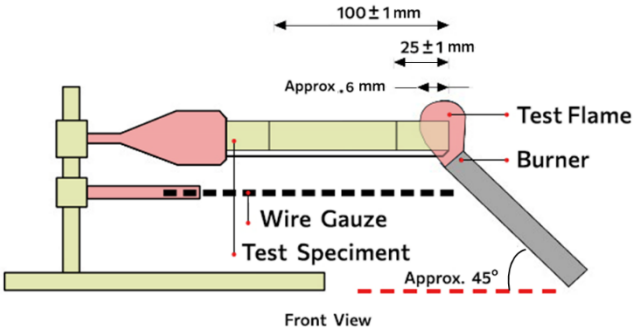

Fig. 3 HBT set-up based on UL94 standard

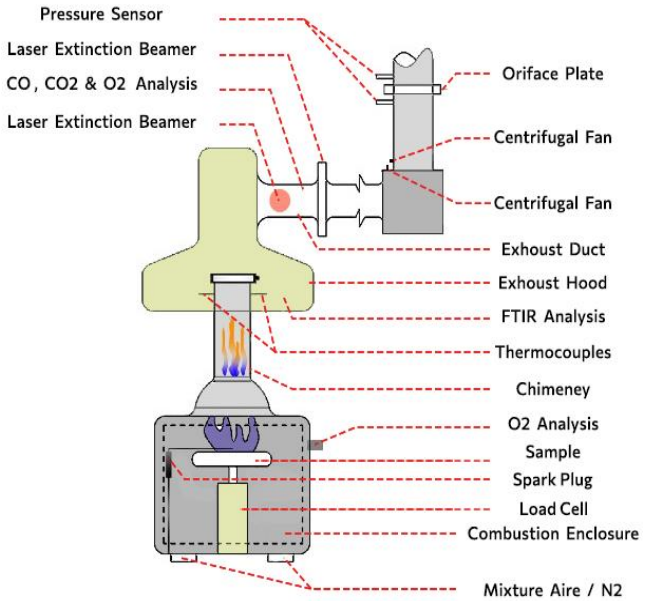

Fig. 4 Scheatic diagram of fire testing based on CCT

turned on when the combustion front reached the 25 mm mark to measure the time for the flame to spread to the benchmark.

2.2.2 Cone Calorimeter Test

The cone calorimeter is often regarded as the most significant bench-scale instrument for fire testing of solid materials (Zhang *et al*. 2019). This device has been also approved by the International Organization for Standardization (ISO5660-1). A schematic diagram of fire testing by CCT is also depicted in Fig. 4. The horizontal dimensions of the sample were (100 ± 1) mm 9 (100 ± 1) mm, while its the thickness was 3 mm. The tests were conducted at atmospheric ambient with sufficient ventilation. The edges and back of the specimens were covered by aluminum foil. The specimen was then placed in a metal plate with a ceramic fiber bed to reduce the effect of heat loss on its back. The distance between the vertex of the specimen and cone heater was 25 mm. The heat flux was 50 kW m^2. The parameters such as MARHE, HRR, TSR, THR, TSP, and ML during combustion were addressed.

2.2.3 Dilatometry

Dilatometry measures the dimensional change of a substance by temperature under negligible load and a specified atmosphere. Dilatometry test is utilized to determine the CTE of the composites. To this end, the samples were cut into cylinders or rectangular cubes with a length of 2-5 cm and a thickness of 3-10 mm. The samples should be cut in such a way that its two sides remain fully flat to be in proper contact with the pushing rod and the end of the ceramic base. According to Fig. 5, the sample is first placed on a ceramic base made of alumina or quartz. At the end of the specimen, a rod transmits the changes in its expansion to the computer to read the displacement. A thermocouple is placed near the sample to measure the temperature. The furnace heats the sample at a certain heating rate, then, the length variations are recorded as a function of temperature.

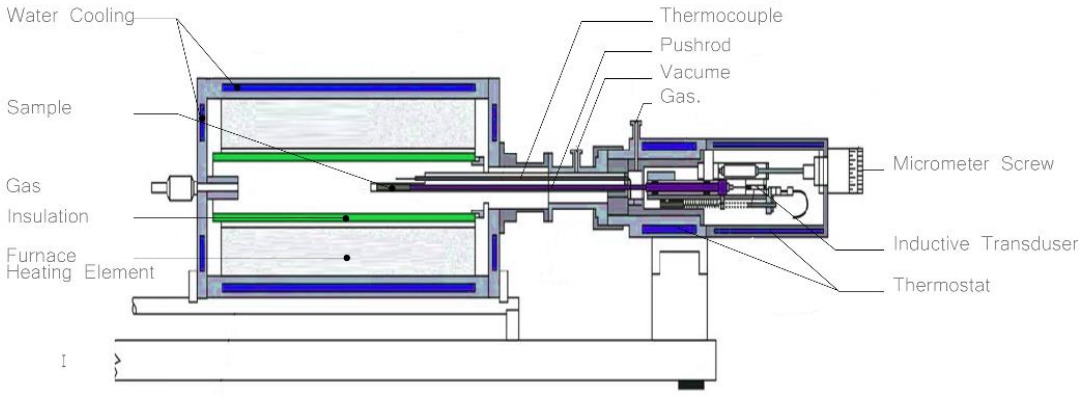

Fig. 5 Schematic diagram of dilatometry instrument

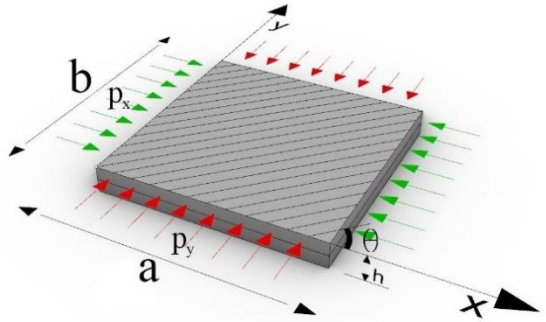

Fig. 6 Schematic of a rectangular composite plate exposed to thermal environment and subjected to mechanical compressive loads

2.2.4 Tensile Test

Tensile test was performed based on ASTM D3039 standard using a universal testing machine (Instron, USA - Load cell capacity ranges from 5N to 5MN). A 2.5-ton load cell was employed in the tensile test of the samples measuring 75 mm in length and 10 mm at its widest section. The crosshead speed was also set at 2 mm/min.

2.3 Thermal stability of composite plates

2.3.1 Stability equilibrium equations

In this subsection, the governing equations for thermal buckling of composite plates are derived. Although the composite systems in the present study consist of short AF, PP, ESP and HNT, the stability equations are provided here in the general form for rectangular composite plates with symmetric cross-ply lay-ups in order to verify the numerical results. First, consider a rectangular laminated plate with thickness h in z direction, length a in x- direction and $b$in y-direction that is under compressive loads as shown in Fig. 6.

Based on FSDT, the displacement components (u, v and w) of the plate may be defined as (Reddy 2003)

$$\begin{aligned} u(x,y,z) &= u_0(x,y) + z\,\phi_x(x,y) \\ v(x,y,z) &= v_0(x,y) + z\,\phi_y(x,y) \\ w(x,y,z) &= w_0(x,y) \end{aligned} \tag{1}$$

where u_0 and v_0 are the displacements of middle surface in the x and $y$directions, w_0 is the transverse deflection, and ϕ_x and ϕ_y are the rotations of the middle surface of the plate about$y$and$x$axes, respectively. The linear strain components associated with the displacements introduced in Eq. (1) are defined as (Reddy 2003)

$$\begin{Bmatrix} \varepsilon_{xx} \\ \varepsilon_{yy} \\ \gamma_{yz} \\ \gamma_{xz} \\ \gamma_{xy} \end{Bmatrix} = \begin{Bmatrix} \varepsilon_{xx}^0 \\ \varepsilon_{yy}^0 \\ \gamma_{yz}^0 \\ \gamma_{xz}^0 \\ \gamma_{xy}^0 \end{Bmatrix} + z \begin{Bmatrix} \varepsilon_{xx}^{(1)} \\ \varepsilon_{yy}^{(1)} \\ \gamma_{yz}^{(1)} \\ \gamma_{xz}^{(1)} \\ \gamma_{xy}^{(1)} \end{Bmatrix}$$
$$= \begin{Bmatrix} \dfrac{\partial u_0}{\partial x} \\ \dfrac{\partial v_0}{\partial y} \\ \dfrac{\partial w_0}{\partial y} + \phi_y \\ \dfrac{\partial w_0}{\partial x} + \phi_x \\ \dfrac{\partial u_0}{\partial y} + \dfrac{\partial v_0}{\partial x} \end{Bmatrix} + z \begin{Bmatrix} \dfrac{\partial \phi_x}{\partial x} \\ \dfrac{\partial \phi_y}{\partial y} \\ 0 \\ 0 \\ \dfrac{\partial \phi_x}{\partial y} + \dfrac{\partial \phi_y}{\partial x} \end{Bmatrix} \tag{2}$$

The constitutive law for the plate under thermal loads is defined as follow (Reddy 2003)

$$\begin{bmatrix} \sigma_{xx} \\ \sigma_{yy} \\ \tau_{yz} \\ \tau_{xz} \\ \tau_{xy} \end{bmatrix} = \begin{bmatrix} \bar{Q}_{11} & \bar{Q}_{12} & 0 & 0 & \bar{Q}_{16} \\ \bar{Q}_{12} & \bar{Q}_{22} & 0 & 0 & \bar{Q}_{26} \\ 0 & 0 & \bar{Q}_{44} & 0 & 0 \\ 0 & 0 & 0 & \bar{Q}_{55} & 0 \\ \bar{Q}_{16} & \bar{Q}_{26} & 0 & 0 & \bar{Q}_{66} \end{bmatrix} \begin{bmatrix} \varepsilon_{xx} \\ \varepsilon_{yy} \\ \varepsilon_{yz} \\ \varepsilon_{xz} \\ \varepsilon_{xy} \end{bmatrix} \tag{3}$$

where$\overline{Q}_{ij}$denote the reduced stiffness coefficients (Reddy 2003). The governing stability equations in the present study are obtained using energy method (Reddy 2003), as follows

$$\delta(U + W) = 0 \tag{4}$$

where U and W represent the total strain energy and the total work of external loads. It should be noted that the effects of thermal stresses as well as the compressive loads appear as external load work in the present study. The strain

energy of the structures is obtained as follows (Li and Yu 2015)

$$\begin{aligned} U = {} & \frac{1}{2}\int_0^a\int_0^b\int_{-\frac{h}{2}}^{\frac{h}{2}}\sigma_x\varepsilon_x dzdydx \\ & + \int_0^a\int_0^b\int_{-\frac{h}{2}}^{\frac{h}{2}}\sigma_y\varepsilon_y dzdydx \\ & + \int_0^a\int_0^b\int_{-\frac{h}{2}}^{\frac{h}{2}}\tau_{xy}\gamma_{xy} dzdydx \\ & + \int_0^a\int_0^b\int_{-\frac{h}{2}}^{\frac{h}{2}}\tau_{xz}\gamma_{xz} dzdydx \\ & + \int_0^a\int_0^b\int_{-h/2}^{h/2}\tau_{yz}\gamma_{yz} dzdydx \end{aligned} \tag{5}$$

The total work done by the external loads, namely thermal loads (N_x^T and N_y^T) and mechanical loads (P_x and P_y) can be calculated by (Li and Yu 2015)

$$\begin{aligned} W = W_{thermal} + W_{mechanical} & \\ = \int_0^a\int_0^b\left(-N_x^T\frac{\partial^2 w}{\partial x^2} - N_y^T\frac{\partial^2 w}{\partial y^2}\right) & \\ + \int_0^a\int_0^b\left(-P_x\frac{\partial^2 w}{\partial x^2} - P_y\frac{\partial^2 w}{\partial y^2}\right) & \end{aligned} \tag{6}$$

where N_x^T and N_y^T are defined as follows

$$\begin{aligned} \begin{Bmatrix} N_x^T, M_x^T \\ N_y^T, M_y^T \\ N_{xy}^T, M_{xy}^T \end{Bmatrix} = \int_{-\frac{h}{2}}^{\frac{h}{2}} & \begin{bmatrix} \overline{Q}_{11} & \overline{Q}_{12} & \overline{Q}_{16} \\ \overline{Q}_{12} & \overline{Q}_{22} & \overline{Q}_{26} \\ \overline{Q}_{16} & \overline{Q}_{26} & \overline{Q}_{66} \end{bmatrix} \\ & \begin{bmatrix} \alpha_{11}\cos^2\theta + \alpha_{22}\sin^2\theta \\ \alpha_{11}\sin^2\theta + \alpha_{22}\cos^2\theta \\ 2(\alpha_{11}-\alpha_{22})\sin\theta\cos\theta \end{bmatrix} \Delta T(1,z)dz \end{aligned} \tag{7}$$

where α_{ij}, ΔT, and θ represent the reduced stiffness coefficients, CTE, temperature difference relative to the reference temperature, and the angle that the long fibers make with *x*-directions, respectively. By inserting Eqs. (6 and 7) into Eq. (5), the following out-of-plane equations may be obtained for rectangular composite plates with symmetric cross-ply lay-ups.

$$\begin{aligned} & D_{11}\left(\frac{\partial^2\varphi_x}{\partial x^2}\right) + D_{12}\left(\frac{\partial^2\varphi_y}{\partial x\partial y}\right) + D_{66}\left(\frac{\partial^2\varphi_x}{\partial y^2} + \frac{\partial^2\varphi_y}{\partial x\partial y}\right) \\ & \qquad - k_sA_{55}\left(\varphi_x + \frac{\partial w}{\partial x}\right) = 0 \\ & D_{66}\left(\frac{\partial^2\varphi_y}{\partial x^2} + \frac{\partial^2\varphi_x}{\partial x\partial y}\right) + D_{12}\left(\frac{\partial^2\varphi_x}{\partial x\partial y}\right) + D_{22}\left(\frac{\partial^2\varphi_y}{\partial y^2}\right) \\ & \qquad - k_sA_{44}\left(\varphi_y + \frac{\partial w}{\partial y}\right) = 0 \\ & k_sA_{55}\left(\frac{\partial\varphi_x}{\partial x} + \frac{\partial^2 w}{\partial x^2}\right) + k_sA_{44}\left(\frac{\partial\varphi_y}{\partial y} + \frac{\partial^2 w}{\partial y^2}\right) \\ & -(P_x + N_x^T)\frac{\partial^2 w}{\partial x^2} - \left(P_y + N_y^T\right)\frac{\partial^2 w}{\partial y^2} = 0 \end{aligned} \tag{8}$$

in which A_{ij} and D_{ij} are the transformed stiffness coefficients defined as

$$(\boldsymbol{A_{ij}, D_{ij}}) = \int_{-\boldsymbol{h/2}}^{\boldsymbol{h/2}\int} \bar{\boldsymbol{Q}}_{\boldsymbol{ij}}(\mathbf{1}, \boldsymbol{z^2})\, \boldsymbol{dz} \tag{9}$$

Furthermore, k_s in Eq. (8) refers to the shear correction factor that is taken here as $5/6$ (Reddy 2003). Simply supported boundary conditions are considered here which are stated as

$$\begin{aligned} & w = 0, \varphi_y = 0, D_{11}\frac{\partial\varphi_x}{\partial x} + D_{12}\frac{\partial\varphi_y}{\partial y} = 0, atx = 0, a \\ & w = 0, \varphi_x = 0, D_{12}\frac{\partial\varphi_x}{\partial x} + D_{22}\frac{\partial\varphi_y}{\partial y} = 0, aty = 0, b \end{aligned} \tag{10}$$

An analytical solution is proposed in the form of:

$$\begin{aligned} w(x,y) &= \sum_{m,n} W_{mn}\sin\frac{m\pi}{a}x\sin\frac{n\pi}{b}y \\ \varphi_x(x,y) &= \sum_{m,n} \Psi_{1mn}\cos\frac{m\pi}{a}x\sin\frac{n\pi}{b}y \\ \varphi_y(x,y) &= \sum_{m,n} \Psi_{2mn}\sin\frac{m\pi}{a}x\cos\frac{n\pi}{b}y \end{aligned} \tag{11}$$

where *m* and *n* denote the number of half-waves in *x* and *y*-directions. The suggested solution satisfies the boundary conditions of Eq. (10). After inserting Eq. (11) into Eq. (8), the following equation is obtained.

$$\begin{bmatrix} K_{11} & K_{12} & K_{13} \\ K_{21} & K_{22} & K_{23} \\ K_{31} & K_{32} & K_{33} \end{bmatrix}\begin{bmatrix} W_{mn} \\ \Psi_{1mn} \\ \Psi_{2mn} \end{bmatrix} = \begin{bmatrix} 0 \\ 0 \\ 0 \end{bmatrix} \tag{12}$$

where K_{ij} are can be found as:

$$\begin{aligned} K_{11} &= \left(k_sA_{55} - (P_x + N_x^T)\right)\left(\frac{m\pi}{a}\right)^2 \\ &+ \left(k_sA_{44} - \left(P_y + N_y^T\right)\right)\left(\frac{n\pi}{b}\right)^2 \\ K_{22} &= D_{11}\left(\frac{m\pi}{a}\right)^2 + D_{66}\left(\frac{n\pi}{b}\right)^2 + k_sA_{55} \\ K_{33} &= D_{66}\left(\frac{m\pi}{a}\right)^2 + D_{22}\left(\frac{n\pi}{b}\right)^2 + k_sA_{44} \\ K_{12} &= K_{21} = \left(\frac{m\pi}{a}\right)k_sA_{55} \\ K_{13} &= K_{31} = \left(\frac{n\pi}{b}\right)k_sA_{44} \\ K_{23} &= K_{32} = (D_{12} + D_{66})\left(\frac{m\pi}{a}\right)\left(\frac{n\pi}{b}\right) \end{aligned} \tag{13}$$

Now, a nontrivial solution is sought for Eq. (13).

$$det\begin{bmatrix} K_{11} & K_{12} & K_{13} \\ K_{21} & K_{22} & K_{23} \\ K_{31} & K_{32} & K_{33} \end{bmatrix} = 0 \tag{14}$$

Solving Eq. (14) yields the following relation

$$\Delta T_{cr} = \frac{f_1 - f_2}{f_3} \tag{15}$$

where

$$\begin{aligned} f_1 &= (k_sA_{55} - P_x)(\frac{m\pi}{a})^2 + \left(k_sA_{44} - P_y\right)(\frac{n\pi}{b})^2 \\ f_2 &= (k_{12}^2k_{33} + k_{13}^2k_{22} - 2k_{12}k_{13}k_{23})/(k_{22}k_{33} - k_{23}^2) \end{aligned} \tag{16}$$

$$f_3 = (\frac{m\pi}{a})^2 \tilde{N}_x^T + (\frac{n\pi}{b})^2 \tilde{N}_y^T$$
$$\begin{pmatrix} \tilde{N}_x^T \\ \tilde{N}_y^T \end{pmatrix} = \int_{-h/2}^{+h/2} \begin{bmatrix} \bar{Q}_{11} & \bar{Q}_{12} \\ \bar{Q}_{12} & \bar{Q}_{22} \end{bmatrix} \begin{Bmatrix} \alpha_x \\ \alpha_y \end{Bmatrix} dz$$

The buckling temperatures of the structure are calculated for different values of *m* and *n*. The minimum obtained value is considered as the critical buckling temperature, denoted by the symbol of ΔT_{cr}.

2.3.2 Verification study

Here, two comparative examples were provided to show the accuracy of the proposed closed-form solution. In the first example, the buckling temperatures of a square composite plate were studied and the results of the present study were compared with those in the literature. The thermo-mechanical properties of this example are assumed to be as follows:

$$E_1 = 15E_2\,,\ E_3 = E_2\,,\ G_{12} = G_{13} = 0.5E_2\,,$$
$$G_{23} = 0.3356\,,\ \upsilon_{12} = \upsilon_{13} = 0.3$$
$$\alpha_1 = 0.015\alpha_0\,,\ \alpha_2 = \alpha_3 = \alpha_0\,,\ \alpha_0 = 10^{-6}/^oC$$

The non-dimensional critical buckling temperatures of the structure were obtained for two thickness-to-width ratios. Table 1 compares the results of the present study with the findings of finite element method (FEM) by Kant and Babu (2000) and generalized differential quadrature method (GDQM) by Kamarian *et al*. (2017). Based on Table 1, the proposed closed-solution of Eq. (15) can accurately predict the buckling temperature of composite plates with the maximum difference of about 1%.

In the second example, the variations of ΔT_{cr} of a square composite plate are provided versus compressive load. The plate is assumed to be subjected to equal compressive load in the *x* and *y* directions ($P_c = P_x = P_y$). As expected, the value of ΔT_{cr} gradually decreased with P_c enhancement. According to Fig. 7, $P_c = 10.931kN/m$ may lead to buckling in the structure even if no thermal stress is generated in the structure. Reddy (2003) obtained similar results ($P_x = P_y = 10.958kN/m$) for the critical mechanical buckling load of the composite plates in the absence of thermal loads. Therefore, Eq. (15) is accurate enough to handle the stability analysis of the composite plates in the present study.

$$\begin{pmatrix} E_1 = 25E_2\,,\ E_3 = E_2\,,\ G_{12} = G_{13} = 0.5E_2\,, \\ G_{23} = 0.2\,,\ \upsilon_{12} = \upsilon_{13} = 0.25\,,\ \alpha_1 = 3\alpha_2 \\ a = b\,,\ a/h = 25\ ,\ P_c = P_x = P_y \end{pmatrix}$$

3. Results and discussion

3.1 Optimal AF/PP composites

First, an optimal combination of AF and PP (OAP) was obtained for the base composite. The first parameter to be measured is the rate of burning which can be determined based on HBT (see Fig. 8). PP is a petroleum-based compound with vigorous flammability capable of producing smoke and toxic substances such as hydrogen halides. On the other hand, high flammability of natural fibers can be

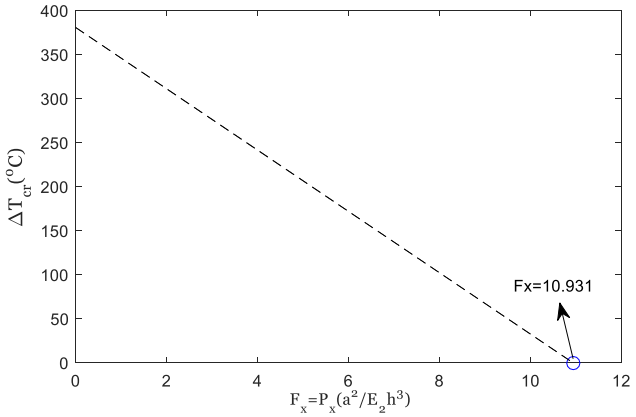

Fig. 7 The variations of non-dimensional buckling temperature ($\overline{\Delta T}_{cr} = 100\Delta T_{cr}\alpha_0$) of a square composite plate versus mechanical compressive load

Table 1 the variations of non-dimensional buckling temperature ($\overline{\Delta T}_{cr}$) of a square ($a = b$) composite plate

		Method		
h/b	$\overline{\Delta T}_{cr}$	Analytical (Present)	GDQM (Kamarian *et al*. 2017)	FEM (Kant and Babu 2000)
0.01	$100\Delta T_{cr}\alpha_0$	0.0996	0.0997	0.0996
0.1	$\Delta T_{cr}\alpha_0$	0.0778	-	0.0770

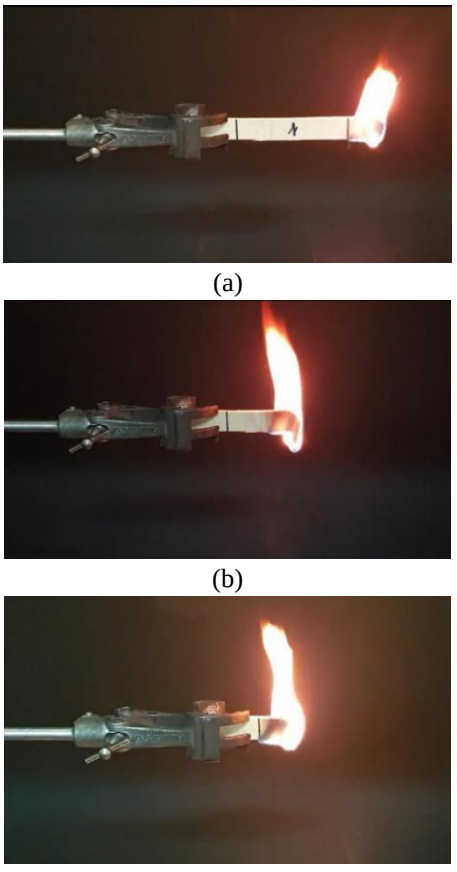

(a) (b) (c)

Fig. 8 Schematic representation of a specimen under HBT: (a) Initial reference point, (b) 150s after ignition, and (c) terminal reference point

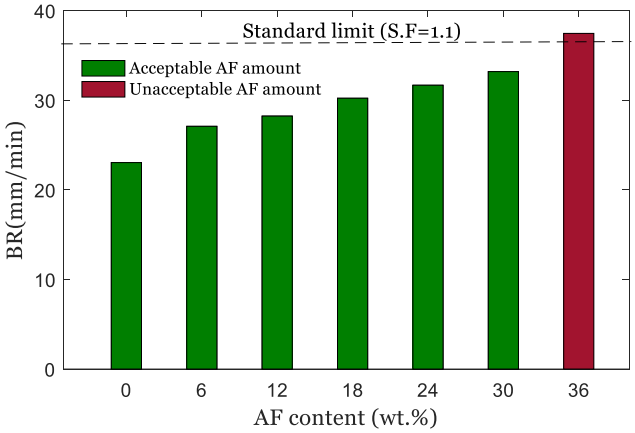

Fig. 9 HBT results for the BR of PP/AF composites at different AF content from 0 to 36 wt.%

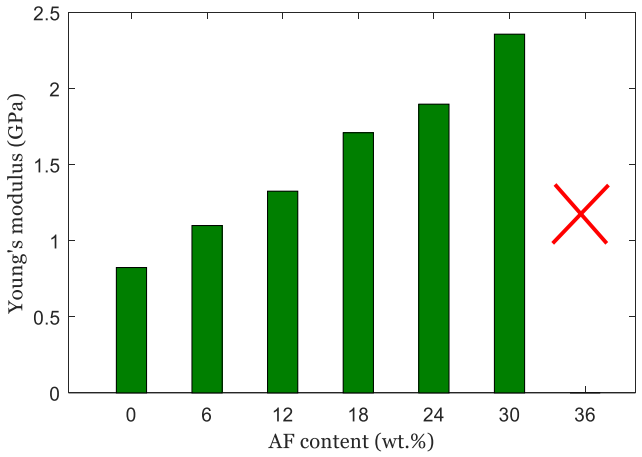

Fig. 10 Young's modulus of AF/PP composites at different AF contents from 0 to 30 wt.%

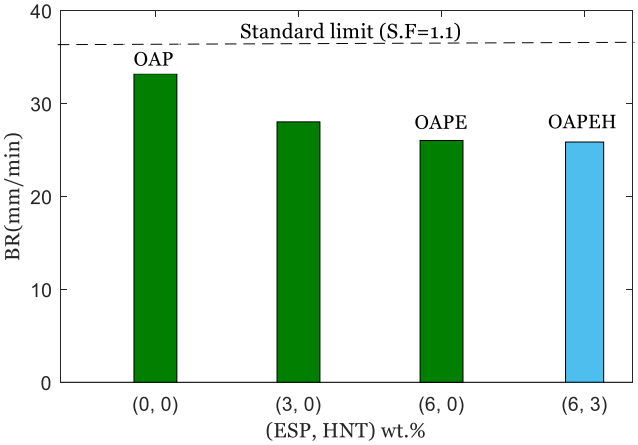

Fig. 11 The effects of ESP and HNT loadings on the BR of the base composite

assigned to their lignin content. For instance, AF includes 60, 24, and 13% cellulose, hemicellulose, and lignin, respectively. As mentioned in Section 2.2.1, the UL94 standard suggests that the BR should be below 40mm/min. However, a safety factor (S.F) of 1.1 is considered here to compensate for the possible and unpredictable errors,

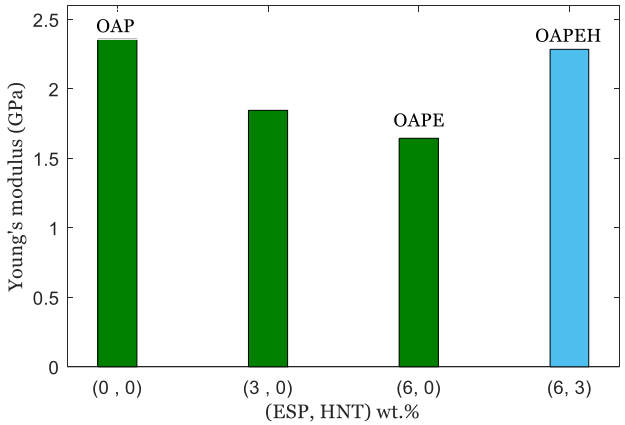

Fig. 12 The effects of ESP and HNT loadings on the Young's modulus of the base composite

Table 2 The combinations of three main composites

Sample code	Combination	Young's modulus (GPa)	BR (mm/min)
OAP	30 wt.% AF+70 wt.% PP	2.36	31.7
OAPE	OAP+6 wt.% ESP	1.68	28.1
OAPEH	OAP+6 wt.% ESP+ 3 wt.% HNT	2.29	27.6

leading to maximum allowed BR value of 36.36 mm/min. The HBT results can be found in Fig. 9. Accordingly, the fire resistance of the composites gradually decreased with enhancing AF content from 0 to 36 wt.%. For the case with 36 wt.% AF, the burning rate exceeds the permissible limit. Therefore, the maximum allowed AF content is 30 wt.%. In the next step, tensile test was applied on the composite specimens with different AF contents (0-30 wt.%) to determine the Young's modulus, whose results can be seen in Fig. 10. Moreover, an increase in the AF content from 0 to 30 wt.% incremented the stiffness from 0.82 to 2.36 GPa. According to HBT and tensile test results, the optimum AF content satisfying the HBT standard with the highest stiffness is 30%. Therefore, the OAP sample comprising 70 wt.% PP and 30 wt.% AF is defined as the base composite (See Table 2).

3.2 OAP composites with suitable content of ESP and HNT

3.2.1 OAP/ESP composites

The effect of ESP incorporation on the flammability and stiffness of the OAP composite was investigated. To this end, two composites were fabricated containing 3 and 6 wt.% ESP which were subjected to HBT test. Based on Fig. 11, the BRs of both samples fall within the permissible range (BR<36.36 mm/min) considering the safety factor of 1.1. Furthermore, higher ESP contents resulted in larger flame resistance of the base composite. Bio-waste ESP contains high levels of calcium carbonate (94%) and organic materials (5%). Hence, ESP acts as a flame-retardant filler due to its high calcium carbonate content. During combustion, calcium carbonate decomposes to

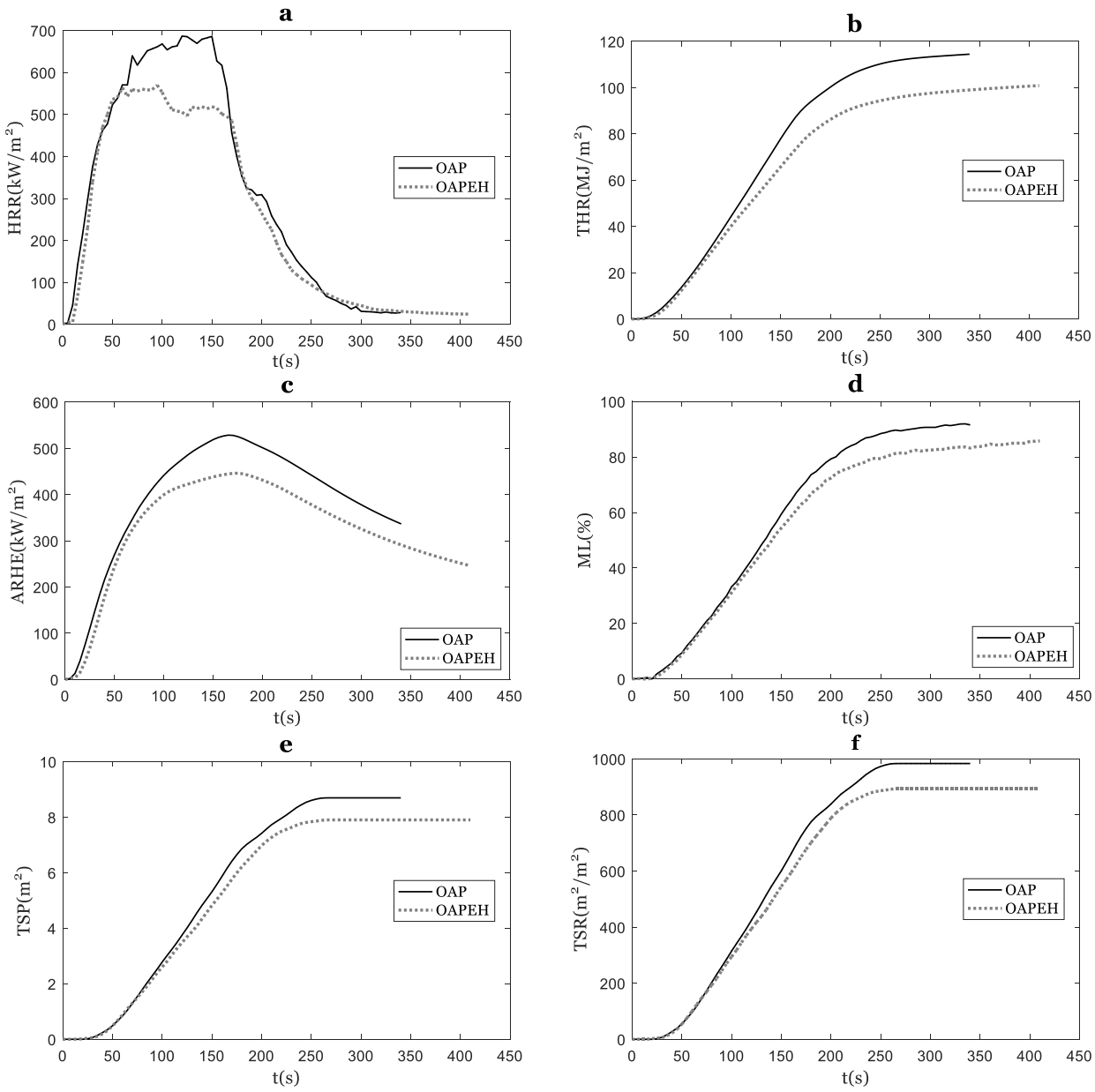

Fig. 13 CCT results for OAP and OAPEH composite samples

liberate carbon dioxide and calcium oxide. The carbon dioxide functions as a diluent, reducing the oxygen concentration in the vicinity of the flame and inhibiting combustion. In addition, the formation of calcium oxide creates a protective layer that functions as a heat barrier, shielding the underlying composite material from the heat source and decreasing the overall combustibility. With this explanation, the experimental results correctly state that 6% ESP can decrease the burning rate of the OAP composite up to 22% (from 33.2 mm/min to 26.0 mm/min). Then, tensile test was performed on the composite samples to obtain the Young's modulus, whose results are demonstrated in Fig. 12. The experimental results showed Young's moduli of 1.85 and 1.65 GPa for the OAP composites containing 3 and 6 wt.% ESP, respectively. Thus, ESP incorporation significantly decreased the stiffness due to the aggregation and poor adhesion between the filler and matrix.

3.2.2 OAP/ESP/HNT composites

Based on previous subsection, although OAP composites containing 6% ESP (i.e. OAPE) showed better fire performance (see Table 2), its stiffness is very poor. In such condition, another eco-friendly additive, called HNT, is suggested to be utilized. It has been shown that an appropriate amount of HNTs can significantly enhance both the mechanical properties and flame resistance of the composites (Kamarian *et al*. 2022). Accordingly, the idea of adding 3% HNT along with 6% ESP into the OAP composite (OAPEH composite, as shown in Table 2) was experimentally explored by measuring its flammability and stiffness using the same experimental setups. It should be noted that the incorporation of HNT provides the composite system with additional flame-retardant properties. During combustion, HNT's unique nanotubular structure assists in the formation of a protective char layer. This layer of char

(a)

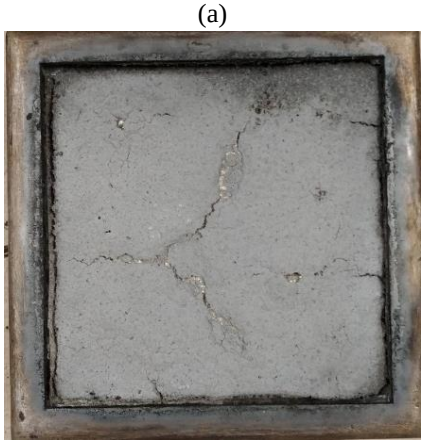

(b)

Fig. 14 Char residue of a) OAP composite and b) OAPEH composite

acts as a physical barrier, preventing further heat transfer and flame spread. In addition to enhancing the barrier effect, the high aspect ratio of HNT promotes the formation of a compact and cohesive char structure. Furthermore, the synergistic effect of ESP and HNT in reducing the flammability of the OAPEH needs to be considered. Through the release of carbon dioxide, ESP contributes to gas phase flame inhibition, whereas HNT enhances char formation and functions as a physical barrier to heat and flame propagation. This combination results in composites with enhanced flame retardancy properties. Figs. 11 and 12 demonstrate the significant role of HNT in the stiffness of OAP composites such that the Young's modulus of OAPEH (2.29 GPa) was close to that of OAP (2.36 GPa). Moreover, the fire resistance of OAPEH was slightly higher than that of OAP. Hence, OAPEH is a proper candidate in the applications requiring both flammability and stiffness.

Cone calorimeter test

As mentioned earlier, HBT is a preliminary fire test which does not provide many details about the performance of the composite upon exposure to flame. Therefore, CCT was applied to make a more accurate and detailed comparison between the flammability of OAP and OAPEH composites. Fig. 13a compares the HRR curves for the samples showing. As seen, the HRR curve of OAPEH is generally lower than that of OAP. The average HRR for the lower curve is about 23.4% less than the other. A remarkable reduction (17.0%) was observed in the peak HRR (from 686.60 kW/m^2 to 569.99 kW/m^2) upon adding 6 wt.% ESP and 3 wt.% HNT. THR is defined as the integral of HRR curves over the duration of the experiment. The experimental results (Fig. 13b) indicated that the THR of the OAPEH composite was 12.1% less than that of the OAP. It means the presence of ESP and HNT may restrict the development of fire. MARHE refers to the maximum average rate of heat emission which can be employed to rank the hazards of developing fires. MAHRE can be defined as the cumulative heat release from t = 0 to time of t per unit of time. The MAHRE can be regarded as an ignition modified rate of heat emission parameter to rank the materials in terms of their ability to measure fire spread to other objects. The experimental results (Fig. 13c) presented the lower MAHRE value for OAPEH composite compared to OAP during the burning time, indicating a reduction in the hazard of fire propagation. Based on the cone calorimetry, the value of MARHE for OAP and OAPEH samples was 528.7 and 446.4 kW/m^2, respectively.

The fourth parameter is mass loss (ML), as illustrated in Fig. 13d. As seen, the difference between the ML curves of OAP and OAPEH gradually increased by time, suggesting that a combination of ESP and HNT acted as a mass transport barrier and slowed down the release of combustible species, thus, reducing the fuel supply of the fire.

Smoke is a common product of almost all fire types, posing a major hazard to life. Smoke particles can decrease visibility due to absorption and scattering of light which may lead to disorientation. Cone calorimeter can be employed to measure the total smoke release (TSR) and total smoke production (TSP). The CCT results showed a significant decrease in both TSR and TSP parameters of the sample containing ESP and HNT. The differences between the curves (Figs. 13e and f) got more prominent over time. The cone calorimeter recorded the TSP of OAP and OAPEH samples as 8.7 and 7.9 m^2, respectively, showing a 9.2 % reduction. Furthermore, the TSR values of the mentioned samples were 983.8 and 893.6 m^2/m^2, respectively.

Figs. 14a and b, which correspond to the char residue analysis, reveal distinct differences in the formation of char between samples containing ESP and HNT and those that do not. In the case of the OAP composites, a stratum of predominantly carbonaceous black and yellow ash can be observed. The presence of fractures within the char layer indicates a relatively weaker structure, permitting the exposure of the layers beneath. In addition, the presence of microscopic openings along the gray ash's perimeter suggests the release of volatile components during combustion. The OAPEH composite, in contrast, has a distinct char morphology. A layer of white carbon covers the surface, indicating a more effective flame-retardant mechanism. In certain areas, a veneer of black ash is visible, indicating the presence of partial combustion. Compared to the OAP composites, the thicker and more cohesive character of the char layer suggests a stronger char formation with less cracking and fragmentation. The limited presence of cracks and microscopic structural holes along

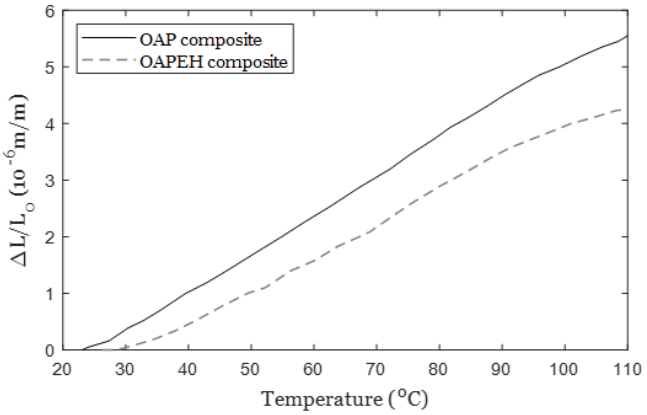

Fig. 15 The variations of the curves $\Delta L/L_0$ versus T obtained from dilatometry experiments

Table 3 Linear CTE of OAP and OAPEH composites

Temperature range	Composite Type		Reduction (%)
	OAP	OAPEH	
$30-70°C$	66.8	54.5	18.4
$70-110°C$	61.0	50.1	17.9
$30-110°C$	63.9	52.3	18.2

Table 4 Thermo-mechanical properties of OAP and OAPEH composites for buckling analysis

Material	Properties		
	$\alpha(\times 10^{-6}/^0C)$	$E(GPa)$	υ
OAP	63.9	2.36	0.3
OAPEH	52.3	2.82	0.3

the perimeter of the OAPEH composites further confirms their enhanced flame retardancy.

The incorporation of ESP and HNT has an effect on the char residue properties of AF/PP composites. The presence of ESP promotes the formation of carbonaceous char, resulting in a structure that is more compact and less fragmented. This is because the decomposition of calcium carbonate releases carbon dioxide, which promotes the formation of a protective char layer. The ESP-containing char has enhanced integrity and reduced porosity, preventing oxygen and heat from reaching the underlying material. Similarly, HNT incorporation contributes to the construction of a cohesive and dense char structure. HNT's nanotubular structure permits the capture of volatile gases and the formation of a stable char network. This prevents heat and flame from penetrating the composite material, providing an additional barrier against the spread of combustion. The co-presence of ESP and HNT in the OAPEH composite leads to a synergistic effect on the char residue. The ESP promotes the formation of carbonaceous char, while the HNT aids in the formation of a compact and cohesive char structure. As a result, the char residue exhibits enhanced structural integrity, decreased fracture, and reduced porosity. This cohesive char layer functions as an insulating barrier, reducing heat transfer and limiting the flame's access to fuel. The observed differences in char residue morphology between OAP and OAPEH composites provide additional evidence for the flame-retardant properties of the latter. Compared to the OAP composites, the white char deposit on the surface of the OAPEH composite indicates a higher degree of carbonization and reduced combustion. The presence of black ash in certain areas indicates localized combustion, but the char layer as a whole remains cohesive and intact.

In general, it can be concluded that the addition of ESP and HNT to AF/PP composites significantly improved their flame retardancy. The ESP acted as a flame-retardant filler by emitting carbon dioxide and forming a protective char layer, while the HNT enhanced the char formation and formed a cohesive barrier against heat and flame propagation.

Dilatometry test

Linear CTEs below the resin glass transition temperature can be calculated from the slope of the curves of $\Delta L/L_0$ versus T obtained from dilatometry test, as shown in Fig. 15. These values are reported in Table 3 for the three temperature ranges of $30-70°C$, $70-110°C$, and $30-110°C$ for OAP and OAPEH composites. As observed, the CTE reduced with the addition of ESP and HNT for all temperature ranges such that the incorporation of 6 wt.% of ESP and 3 wt.% of HNT resulted in an 18% reduction in the CTE.

Critical buckling temperature

The difference between the critical buckling temperatures (ΔT_{cr}) of OAP and OAPEH composite plates is examined in this subsection. The thermo-mechanical properties of the composites are listed in Table 4 based on the experiments discussed in previous Sections 3. Noteworthy, the Poisson's ratio is assumed to be 0.3 for composites made of abaca and PP, according to Vilaseca *et al.* (2010). The length and width of the plate are considered to be $100mm$ while the thickness varies from $5mm$ to $10mm$. The plate is supposed to be exposed to thermal environment with uniform temperature distribution. In addition, it is assumed that the compressive mechanical loads are applied to the plates at the edges. Note that the analysis here is for the cases with equal compressive loads in *x* and *y* directions ($P_x = P_y = P_c$).

Fig. 16 illustrates the variations of ΔT_{cr} against compressive load for OAP and OAPEH composite plates. The results are depicted for two h/b ratios. As can be observed in Fig. 16a, the critical temperature of the OAP composite started at 48.82 °C and gradually decreased with the increase of compressive load until it reaching zero at $P_c = 52.58kN/m$ (i.e. the mechanical buckling point). Fig. 16a also shows the variations of buckling temperature of OAPEH composite versus mechanical load. It is clear that the OAPEH graph is above that of the OAP in a vast majority of temperatures due to the low CTE and almost the same Young's modulus of the base composite in comparison to the sample incorporated with 6%ESP and 3% HNT. The theoretical results represent the significant influence of ESP and HNT additives on the stability of AF/PP composites. When the compressive load is larger than $50kN/m$, however, the OAP composite shows better performance

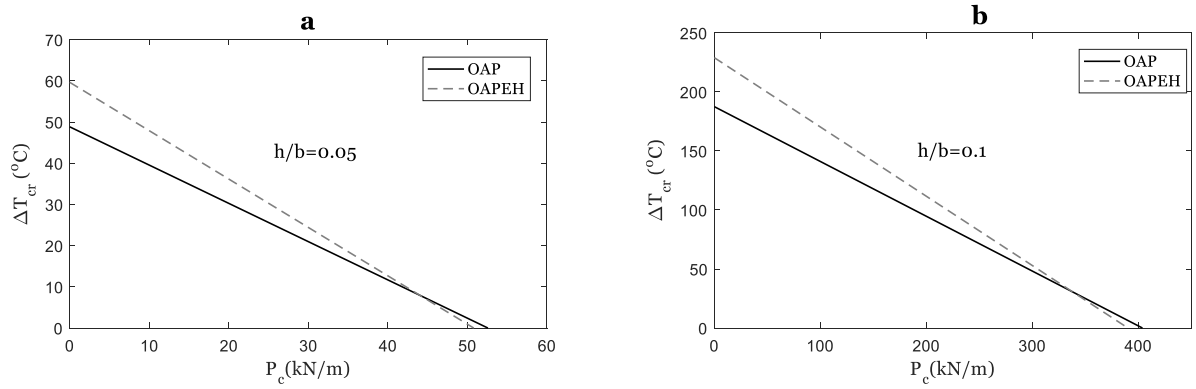

Fig. 16 Critical buckling temperatures of OAP and OAPEH composite plates versus compressive load for a) $h/b = 0.05$ and b) $h/b = 0.1$

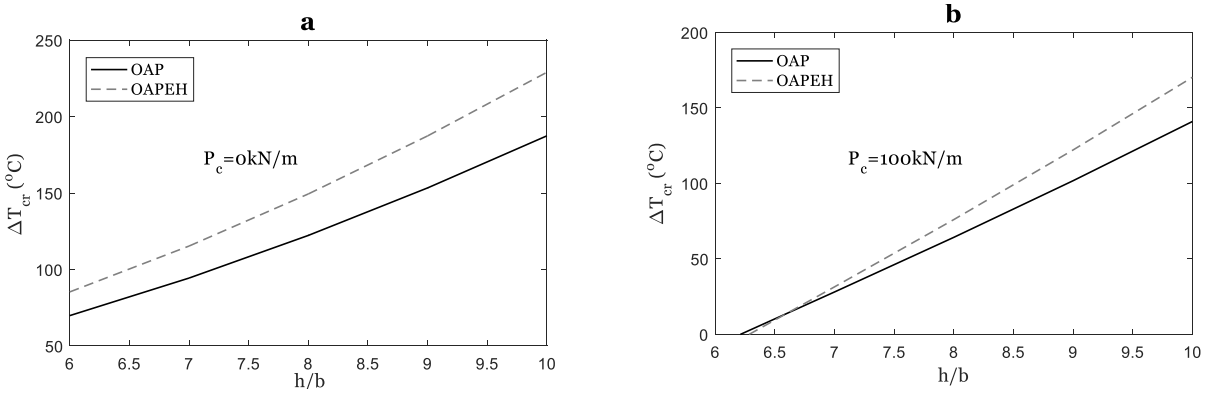

Fig. 17 The variations of critical buckling temperatures of OAP and OAPEH composite plates versus thickness for a) $P_c = 0kN/m$ and b) $P_c = 100kN/m$

than the OAPEH due to its higher Young's modulus. In other words, the negative effect of incorporation of ESP and HNT on the Young's modulus is more prominent than their positive effects on the CTE when P_c is larger than about $43.5kN/m$. Fig. 16b demonstrates similar trends for the bucking temperature of OAP and OAPEH composites against P_c when $h/b = 0.1$. The only difference is the larger values of ΔT_{cr} due to considering a thicker structure. The linear ΔT_{cr} changes in Figs. 16a and b can be due to the constant and temperature-independent values of the thermo-mechanical properties (CTE, Young's modulus and Poisson's ratio) of Table 4.

The influence of ESP and HNT additives on the stability of AF/PP composites are also examined as depicted in Fig. 17. The variations of buckling temperature against thickness-to-width ratio are depicted in Fig. 17a in the absence of mechanical load ($P_c = 0$). As expected, the stiffness of the structure increases with an increment in the h/b ratio which raises the resistance against thermal buckling, delaying the critical temperature. Furthermore, the difference between the curves of OAP and OAPEH increases as the structure gets thicker. Similar results are shown in Fig. 17b for $P_c = 100kN/m$. This case more clearly shows the remarkable effect of ESP and HNT on the stability of composite structures. As an example, the OAP composite structure with a thickness below 6.5 mm buckles even in the absence of temperature elevation, while this critical thickness is 6.3 mm for the ESP/HNT-incorporated sample. However, the difference between the curves gets more profound as the plate becomes thicker, since the OAPEH composite withstands higher temperature before buckling. For instance, when $h = 9mm$, the values of ΔT_{cr} are 101.8 and 122.2 $\circ C$ for OAP and OAPEH composites, respectively.

Noteworthy, Figs. 16 and 17 are presented with no consideration of the limit of the glass transition temperature, which of course does not affect the interpretation of the reported results.

4. Conclusions

An attempt was made in the present work to find an optimal eco-friendly composite composed of AF, PP, ESP, and HNT in terms of the flammability performance and thermal buckling behavior. Therefore, the flammability parameters, thermal expansion coefficient, and mechanical properties were examined as the most important factors. First, an optimal base composite made of AF and PP was introduced according to the data obtained from HBT and tensile test. Accordingly, 30 wt.% AF and 70 wt.% PP led to an optimal base composite. Then, a suitable combination of additives comprising 6 wt.% ESP and 3 wt.% HNT was used to achieve the OAPEH composite. The additives

significantly reduced the BR with no sharp drop in the stiffness of OAP composites. In the next step, CCT was carried out on the OAP and OAPEH samples to attain more details on the performance of the composites in fire. The results indicated a 9~23% decrease in all flammability parameters such as HRR, THR, MARHE, TSP, and TSR upon adding 6 wt.% ESP and 3 wt.% HNT. The resulting char residue of the OAPEH composite had a more compact, less fragmented, and thermally stable structure, indicating that AF/PP composites incorporated with ESP and HNT had enhanced flame-retardant properties. Then, the dilatometry test was carried out to compare the CTE of OAP and OAPEH composites. It was found that the CTE of OAPEH was about 18% lower than that of the base composite. Finally, the influence of ESP and HNT on the thermal stability of OAP composites was analytically discussed. A closed-form solution was developed based on FSDT to estimate the critical buckling temperatures of the composite structures under mechanical compressive load. An optimal combination of ESP and HNT significantly enhanced the buckling resistance of composite structures under thermo-mechanical loads. In short, the results of present study stated that a suitable combination of ESP and HNT can reduce the flammability properties as well as the CTE of eco-friendly PP/AF composites with no significant decline in the mechanical properties.

Acknowledgment

This research was supported by Basic Science Research Program through the National Research Foundation of Korea (NRF) funded by the Ministry of Education (No. 2018R1A6A1A03024509)

References

Balan, G.S., Krishnan, A.M., Saravanavel, S. and Ravichandran, M. (2020), "Investigation of hardness characteristics of waste plastics and egg shell powder reinforced polymer composite by stirring route", *Mater. Today Pr.*, **33**, 4090-4093. https://doi.org/10.1016/j.matpr.2020.06.545.

Barba, B.J.D., Madrid, J.F. and Penaloza Jr, D.P. (2020), "A review of abaca fiber-reinforced polymer composites: Different modes of preparation and their applications", *J. Chilean Chem. Soc.*, **65**(3), 4919-4924. http://doi.org/10.4067/s0717-97072020000204919

Behdinan, K. and Moradi-Dastjerdi, R. (2022), "Thermal buckling resistance of a lightweight lead-free piezoelectric nanocomposite sandwich plate", *Adv. Nano Res.*, **12**(6), 593-603. https://doi.org/10.12989/anr.2022.12.6.593.

Busico, V. and Cipullo, R. (2001), "Microstructure of polypropylene", *Prog. Polym. Sci.*, **26**(3), 443-533. https://doi.org/10.1177/0892705711428659.

Carrera, E., Fazzolari, F.A. and Cinefra, M. (2016), *Thermal Stress Analysis of Composite Beams, Plates and Shells: Computational Modelling and Applications*, Academic Press

Chalapathi, K.V., Song, J.I. and Prabhakar, M. (2022), "Impact of surface treatments and hybrid flame retardants on flammability, and thermal performance of bamboo fabric composites", *J. Natural Fibers*, **19**(6), 2129-2139. https://doi.org/10.1080/15440478.2020.1798849.

Dai, H. and Safarpour, H. (2021), "Frequency and thermal buckling information of laminated composite doubly curved open nanoshell", *Adv. Nano Res.*, **10**(1), 1-14.

Deng, S., Zhang, J., Ye, L. and Wu, J. (2008), "Toughening epoxies with halloysite nanotubes", *Polymer*, **49**(23), 5119-5127. https://doi.org/10.1016/j.polymer.2008.09.027.

Eslami, M. (2010), *Thermo-Mechanical Buckling of Composite Plates And Shells*, Amirkabir University Press, Tehran.

Jena, D.K. and Sahoo, P.K. (2019), "New strategies for the construction of eggshell powder reinforced starch based fire hazard suppression biomaterials with tailorable thermal, mechanical and oxygen barrier properties", *Int. J. Biol. Macromol.*, 140(496-504). https://doi.org/10.1016/j.ijbiomac.2019.08.156.

Jirimali, H.D., Chaudhari, B.C., Khanderay, J.C., Joshi, S.A., Singh, V., Patil, A.M. and Gite, V.V. (2018), "Waste eggshell-derived calcium oxide and nanohydroxyapatite biomaterials for the preparation of LLDPE polymer nanocomposite and their thermomechanical study", *Polym. Plast. Technol. Eng.*, **57**(8), 804-811. https://doi.org/10.1080/03602559.2017.1354221.

Kamarian, S., Shakeri, M. and Yas, M.H. (2017), "Thermal buckling optimisation of composite plates using firefly algorithm", *J. Experim. Theo. Artif. Intell.*, **29**(4), 787-794. https://doi.org/10.1080/0952813X.2016.1259267.

Kamarian, S. and Song, J.I. (2022), "Review of literature on eco-friendly sandwich structures made of non-wood cellulose fibers", *J. Sandw. Struct. Mater.*, **24**(3), 1653-1705. https://doi.org/10.1177%2F10996362211062372.

Kamarian, S., Yu, R. and Song, J.I. (2022), "Synergistic effects of halloysite nanotubes with metal and phosphorus additives on the optimal design of eco-friendly sandwich panels with maximum flame resistance and minimum weight", *Nanotechnol. Rev.*, **11**(1), 252-265. https://doi.org/10.1515/ntrev-2022-0014.

Kang, D.J., Pal, K., Park, S.J., Bang, D.S. and Kim, J.K. (2010), "Effect of eggshell and silk fibroin on styrene–ethylene/butylene–styrene as bio-filler", *Mater. Des.*, **31**(4), 2216-2219. https://doi.org/10.1016/j.matdes.2009.10.033.

Kant, T. and Babu, C.S. (2000), "Thermal buckling analysis of skew fibre-reinforced composite and sandwich plates using shear deformable finite element models", *Compos. Struct.*, **49**(1), 77-85. https://doi.org/10.1016/S0263-8223(99)00127-0

Karunakaran, S., Majid, D. and Tawil, M.M. (2016), "Flammability of self-extinguishing kenaf/ABS nanoclays composite for aircraft secondary structure", *Proceedings of the IOP Conference Series: Materials Science and Engineering*, **152**(1), 012068, IOP Publishing.

Lee, D.W., Kim, S., Kim, B.S. and Song, J.I. (2013), "Tensile and fire retardant properties of nanoclay reinforced Abaca/Polypropylene composite", *Proceedings of the 2013 International Conference on Aerospace Science & Engineering (ICASE)*, IEEE, 1-5.

Li, X. and Yu, K. (2015), "Vibration and acoustic responses of composite and sandwich panels under thermal environment", *Compos. Struct.*, **131**(1040-1049). https://doi.org/10.1016/j.compstruct.2015.06.037.

Li, Z., Shah, A.R., Prabhakar, M. and Song, J.-i. (2017), "Effect of inorganic fillers and ammonium polyphosphate on the flammability, thermal stability, and mechanical properties of abaca-fabric/vinyl ester composites", *Fibers Polym.*, **18**(3), 555-562. https://doi.org/10.1007/s12221-017-6859-7.

Liu, K., Takagi, H. and Yang, Z. (2013), "Dependence of tensile properties of abaca fiber fragments and its unidirectional composites on the fragment height in the fiber stem", *Compos. Part A Appl. Sci.*, **45**, 14-22. https://doi.org/10.1016/j.compositesa.2012.09.006.

Liu, M., Guo, B., Zou, Q., Du, M. and Jia, D. (2008), "Interactions between halloysite nanotubes and 2, 5-bis (2-benzoxazolyl)

thiophene and their effects on reinforcement of polypropylene/ halloysite nanocomposites", *Nanotechnology*, **19**(20), 205709. https://doi.org/10.1088/0957-4484/19/20/205709.

Liu, M., Wu, C., Jiao, Y., Xiong, S. and Zhou, C. (2013), "Chitosan–halloysite nanotubes nanocomposite scaffolds for tissue engineering", *J. Mater. Chem. B*, **1**(15), 2078-2089. https://doi.org/10.1039/C3TB20084A.

Maddah, H.A. (2016), "Polypropylene as a promising plastic: A review", *Am. J. Polym. Sci*, **6**(1), 1-11. https://doi.org/10.5923/j.ajps.20160601.01.

Madsen, B. and Gamstedt, E.K. (2013), "Wood versus plant fibers: similarities and differences in composite applications", *Adv. Mater. Sci. Eng*., 2013. https://doi.org/10.1155/2013/564346.

Mai Nguyen Tran, T., Mn, P., Lee, D.W., Cabo, M., Jr and Song, J.I. (2021), "Polypropylene/abaca fiber eco-composites: Influence of bio-waste additive on flame retardancy and mechanical properties", *Polym. Compos.*, **42**(3), 1356-1370. https://doi.org/10.1002/pc.25906.

Manickavasagam, V., Vijaya Ramnath, B., Elanchezhian, C., Vignesh, V., Vijai Rahul, V., Sathya Narayanan, S. and Tamilselvan, V. (2014), "Investigation on compression and hardness properties of abaca and manila hybrid composite", *Appl. Mech. Mater*., **680**, 23-26.

Massaro, M., Lazzara, G., Milioto, S., Noto, R. and Riela, S. (2017), "Covalently modified halloysite clay nanotubes: synthesis, properties, biological and medical applications", *J. Mater. Chem. B*, **5**(16), 2867-2882. https://doi.org/10.1039/C7TB00316A.

Mouritz, A.P. and Gibson, A.G. (2007), *Fire properties of polymer composite materials*, Springer Science & Business Media.

Naumenko, E.A., Guryanov, I.D., Yendluri, R., Lvov, Y.M. and Fakhrullin, R.F. (2016), "Clay nanotube–biopolymer composite scaffolds for tissue engineering", *Nanoscale*, **8**(13), 7257-7271. https://doi.org/10.1039/C6NR00641H.

Ochi, S. (2006), "Development of high strength biodegradable composites using Manila hemp fiber and starch-based biodegradable resin", *Compos. Part A Appl. Sci.*, **37**(11), 1879-1883. https://doi.org/10.1016/j.compositesa.2005.12.019.

Qiu, J., Jiang, L., Orabi, M.A., Usmani, A. and Li, G. (2022), "A computational approach for modelling composite slabs in fire within OpenSees framework", *Eng. Struct*., **255**(113909). https://doi.org/10.1016/j.engstruct.2022.113909.

Reddy, J.N. (2003), *Mechanics of laminated composite plates and shells: theory and analysis*, CRC press.

Renner, J.S., Mensah, R.A., Jiang, L., Xu, Q., Das, O. and Berto, F. (2021), "Fire behavior of wood-based composite materials", *Polymers*, **13**(24), 4352. https://doi.org/10.3390/polym13244352.

Santos, A.C., Ferreira, C., Veiga, F., Ribeiro, A.J., Panchal, A., Lvov, Y. and Agarwal, A. (2018), "Halloysite clay nanotubes for life sciences applications: From drug encapsulation to bioscaffold", *Adv. Colloid Interf. Sci*., **257**, 58-70. https://doi.org/10.1016/j.cis.2018.05.007.

Shaik, M.S. and Subramanian, H.S. (2021), "An Experimental Investigation on Low-velocity Impact Response of Abaca/ Epoxy Bio-composite", *J. Natural Fibers*, 1-16. https://doi.org/10.1080/15440478.2021.1941485.

Shan, X. and Huang, A. (2022), "Intelligent simulation of the thermal buckling characteristics of a tapered functionally graded porosity-dependent rectangular small-scale beam", *Adv. Nano Res.*, **12**(3), 281-290. https://doi.org/10.12989/anr.2022.12.3.281

Shubhra, Q.T., Alam, A.M. and Quaiyyum, M.A. (2013), "Mechanical properties of polypropylene composites: A review", *J. Thermoplast. Compos. Mater*., **26**(3), 362-391. https://doi.org/10.1016/S0079-6700(00)00046-0.

Sun, R., Fang, J., Goodwin, A., Lawther, J. and Bolton, A. (1998), "Isolation and characterization of polysaccharides from abaca fiber", *J. Agric. Food Chem*., **46**(7), 2817-2822. https://pubs.acs.org/doi/abs/10.1021/jf9710894.

Tsai, W.T., Yang, J.M., Lai, C.W., Cheng, Y.H., Lin, C.C. and Yeh, C.W. (2006), "Characterization and adsorption properties of eggshells and eggshell membrane", *Bioresour. Technol*., **97**(3), 488-493. https://doi.org/10.1016/j.biortech.2005.02.050.

Vasquez, J.Z. and Diaz, L.J.L. (2017), "Unidirectional abaca fiber reinforced thermoplastic starch composite", *Mater. Sci. Forum*, **894**, 56-61.

Vijaya Ramnath, B., Manickavasagam, V., Elanchezhian, C., Santhosh Shankar, A., Sundarrajan, R., Vickneshwaran, S. and Pithchai Pandian, S. (2014), "Investigation on flexural and impact properties of abaca and Manila hybrid composite", *Adv. Mater. Res*., **1051**, 102-106.

Vijayalakshmi, K., Neeraja, C.Y., Kavitha, A. and Hayavadana, J. (2014), "Abaca fibre", *Transact. Eng. Sci*., **2**(9), 16-19

Vilaseca, F., Valadez-Gonzalez, A., Herrera-Franco, P.J., Pèlach, M.À., López, J.P. and Mutjé, P. (2010), "Biocomposites from abaca strands and polypropylene. Part I: Evaluation of the tensile properties", *Bioresour. Technol*., **101**(1), 387-395.

Xu, Z., Chu, Z., Yan, L., Chen, H., Jia, H. and Tang, W. (2019), "Effect of chicken eggshell on the flame-retardant and smoke suppression properties of an epoxy-based traditional APP-PER-MEL system", *Polym. Compos*., **40**(7), 2712-2723. https://doi.org/10.1002/pc.25077.

Zhang, Z., Wang, C., Huang, G., Liu, H. and Zhao, W. (2019), "Thermal decomposition characteristic parameters for the outer material of composite hydrogen storage tank by cone calorimeter", *J. Therm. Anal. Calorim*., **138**, 1299-1310. https://doi.org/10.1007/s10973-019-08189-6.

CC